Multi-Link Multi-Contact Force Control for Manipulators

Jaeheung Park and Oussama Khatib
Artificial Intelligence Laboratory
Stanford University
Stanford, CA 94305, USA
{*park73, ok*}*@robotics.stanford.edu*

***Abstract*— This paper presents a compliant motion control framework for multiple contacts distributed over multiple links. The one link multi-contact control approach implemented in our previous work has been extended to contacts over multiple links. Experimental results demonstrate three point contact control on two links of a PUMA560 manipulator. A robust force control design is implemented with a Kalman estimator and full state feedback method to compensate for the modeling errors of the manipulator and environment.**

***Index Terms*— multiple contact, multiple link, force control, and manipulator**

I. Introduction

In recent years the robotics community has been witnessing the emergence of humanoid robots that are designed to operate in complex human environments. Operating under these conditions inevitably involves complex interactions with the physical environment (see Figure 1). For this reason it is critical to incorporate a robust framework for multi-contact resolution into future controllers.

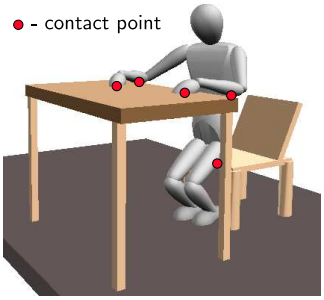

Fig. 1. **Humanoid robot interacting with a complex human environment.** Such interactions involve many contact conditions.

Our previous work [3][8] proposed a multi-contact kinematic model and control structure and demonstrated a successful implementation of multi-contact at the end-effector. This kinematic model is more general than the Raibert-Craig model [9] which provides only an orthogonal decomposition of the operational space. It is noted that other work has also been done which presents a general kinematic contact model [1] [6] [10].

More complex tasks with higher DOF manipulators may involve more contacts on multiple links, rather than contact exclusively at the end-effector. Liu et al. [7] present an adaptive control approach for multiple geometric constraints using joint-space orthogonalization. The joint-space orthogonalization scheme projects the desired joint space velocity, and errors, onto the tangential plane of the geometric surface for joint space motion control. In this manner the contact force control is decoupled from the motion control. Since the projection is on joint space, the geometric constraints can be any function of the joint angles. However, the adaptive hybrid control approach used in this scheme does not provide a decoupled control structure for each contact, although it does guarantee convergence to the desired contact forces. Also, a model of the contact environment is not included in the control design.

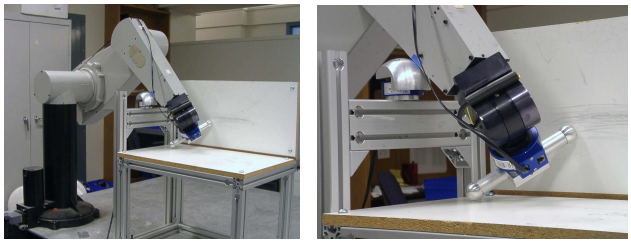

Fig. 2. **PUMA560 having three contacts**

This paper presents a multiple contact force control scheme for multiple links using the operational space formulation. Control points (operational points) are chosen at the links that will be in contact with the environment. The multi-contact model [3] divides the space of each control point into a contact normal space and a free motion space. The composition of the contact normal spaces on the multiple links defines the operational space coordinates. The contact environment model is then incorporated into the operational space framework, resulting in a decoupled linear second-order system for each contact force.

Contact force control based on this framework utilizes an Active Observer (AOB) [2] based on a modified Kalman filter. The AOB is applied to the decoupled sub-system that is derived from the multi-contact model and operational space formulation. This strategy greatly simplifies the control structure and provides a high level of robustness.

Experiments were conducted on a PUMA560 manipulator to demonstrate our multi-contact and multi-link approach. Three points were in contact with the environment: one on the third link and two on the end-effector (Figure 2). The experiments were conducted with and without null space motion. This is, to our knowledge, the first demonstration of multi-contact force control on multiple links. Additionally, our implementation provides a decoupled structure for multi-contact control.

II. Formulation

For the lth link having r contacts with environment, the free motion space and contact normal space with respect to the control point of the link can be described by[1] [3]

$$\vartheta^l_{c.p.} = T^l_t \beta^l_t \quad (1)$$

$$f^l_{c.p.} = N^l_c f^l_c, \quad (2)$$

where $\vartheta^l_{c.p.}$ is the free motion space velocity of the control point, which does not disturb the contact forces. The term $f^l_{c.p.}$ is the force at the control point due to the contact forces and f^l_c is the vector of r contact forces. The dimensions of $f^l_{c.p.}$ and f^l_c are 6 and r, respectively. The matrix T^l_t spans the free motion space and N^l_c spans the contact normal space. We note that N^l_c and T^l_t are orthogonal to each other, i.e. ${N^l_c}^T T^l_t = 0$. These spaces and matrices are described at the control point of the link that has contact with environment; thus, the dimension of N^l_c and T^l_t are $6 \times r$ and $6 \times (6-r)$.

To achieve contact force control, the control force has to be applied in the space of N^l_c and the desired motion has to be designed in T^l_t for the corresponding control point. The implementation of this multi-contact force control is accomplished with projection matrices when only one link has contact with environment. The dynamic equations for the control point of the link can be modeled with the operational space formulation [8].

However, when multiple links have contacts with environment, multiple control points on the individual links have to be chosen to describe contacts using contact normal spaces. Therefore, the use of projection matrices for control points is no longer as straightforward as in the case of a single control point. A better approach is to define the operational space coordinates to be the displacements in the contact normal spaces.

A. Operational Space Coordinates

Equation (2) provides the contact normal space matrix, N^l_c, for the contacts on the lth link. The operational space coordinates are defined to be the displacements in the contact normal spaces, N^l_c. The instantaneous velocity of the coordinates will be denoted as ϑ^l_c. The Jacobian for these coordinates is

$$J^l_c = {N^l_c}^T J^l, \quad (3)$$

where J^l is the Jacobian for the control point of the lth link.

For n link contacts, the Jacobian is obtained by constructing the composition of these Jacobians for each link.

$$J_c = \begin{pmatrix} J^l_c \\ J^{l+1}_c \\ \vdots \\ J^{l+n-1}_c \end{pmatrix}. \quad (4)$$

[1]To clearly distinguish contact forces, f^l_c, from the measured contact force/moment at the control point, $f^l_{c.p.}$, some of the notations are changed from those in [3]. Also, subscript c is introduced to the contact normal space matrix, N^l_c, to differentiate it from the null space projection matrix, N^T_0, which will be introduced in the following subsection.

Similarly, a concatenation of ϑ^l_c vectors forms the instantaneous velocity of the operational space coordinate, ϑ_c, and a concatenation of f^l_c forms contact force vector, f_c.

B. Control Structure

The equations of motion for manipulators are

$$A(q)\ddot{q} + b(q,\dot{q}) + g(q) + J_c(q)^T f_c = \Gamma, \quad (5)$$

where q is the vector of joint space coordinates. Γ is the vector of joint torques. $A(q)$ is the joint space inertia matrix. $b(q,\dot{q})$ is the vector of Coriolis and centrifugal terms. $g(q)$ is the vector of gravity terms.

The joint torques, Γ, is chosen to be composed of the torque for contact force control and null space torque [4];

$$\Gamma = J^T_c F_c + N^T_0 \Gamma_0. \quad (6)$$

The equation of motion for ϑ_c is then

$$\Lambda_c(q)\dot{\vartheta}_c + \mu_c(q,\dot{q}) + p_c(q) + f_c = F_c, \quad (7)$$

where

$$\Lambda^{-1}_c(q) = J_c(q)A(q)^{-1}J_c(q)^T \quad (8)$$

$$\bar{J}^T_c(q) = \Lambda_c(q)J_c(q)A(q)^{-1} \quad (9)$$

$$N^T_0 = I - J^T_c \bar{J}^T_c \quad (10)$$

$$\mu_c(q,\dot{q}) = \bar{J}_c(q)^T b(q,\dot{q}) - \Lambda_c(q)\dot{J}(q)\dot{q} \quad (11)$$

$$p_c(q) = \bar{J}_c(q)^T g(q). \quad (12)$$

The control force, F_c, in Equation (7) can be designed by compensating the dynamic effects with the estimates of the matrices, $\hat{\Lambda}_c(q)$, $\hat{\mu}_c(q,\dot{q})$, $\hat{p}_c(q)$, and $\hat{f}_c$[2].

$$F_c = \hat{\Lambda}_c(q)f^*_c + \hat{\mu}_c(q,\dot{q}) + \hat{p}_c(q) + \hat{f}_c. \quad (13)$$

The resulting equations of motion form the decoupled unit mass system for each contact.

$$\dot{\vartheta}_c = f^*_c. \quad (14)$$

$$\text{i.e.} \quad \dot{\vartheta}_{c,i} = f^*_{c,i}, \quad (15)$$

where i denotes each contacts.

The null space control torque, Γ_0, is used for motion control. The dynamically consistent null space projection matrix, N^T_0, projects the torque, Γ_0, into the null space of the contact forces; thus, the contact forces are not affected by Γ_0.

III. Contact Environment Model and Contact Force Control Design

Designing the contact force controller requires knowledge of the contact environment. A precise model of the environment is hard to construct; thus, a robust controller is designed to deal with modeling errors while a simple environment model is used.

The contact environment model used in our experiments is a spring model [5], in which the environment is assumed to have a constant stiffness. For each contact i,

$$\dot{f}_{c,i} = k_{s,i}\vartheta_{c,i}, \quad (16)$$

[2]The estimate of f_c is the result from the Kalman estimator, which is explained in Section III.

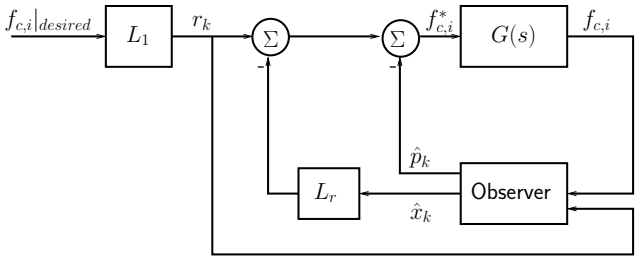

Fig. 3. **Force Control Design.** $G(s)$ is the system transfer function from the command $f^*_{c,i}$ to the contact force $f_{c,i}$. The term $f_{c,i}|_{desired}$ is the desired contact force. The terms r_k, $\hat{x}_k$, and $\hat{p}_k$ are reference input, state estimate, and input error estimate. L_r and L_1 are a full state feedback gain and a scaling factor to compute reference input r_k.

where $f_{c,i}$ is the ith contact force. The term $\vartheta_{c,i}$ is the instantaneous velocity in the contact normal direction. The term $k_{s,i}$ is the ith contact environment stiffness.

With this model and Equation (15), the equations of motion for each contact i, that are to be used for control design, are

$$\ddot{f}_{c,i} = k_{s,i} f^*_{c,i}. \tag{17}$$

A. Force Controller

Force control design starts with Equation (17), which is the second order dynamic equation for each contact force. After adding additional damping[3], the system transfer function from the command, $f^*_{c,i}$, to the contact force, $f_{c,i}$, can be derived as

$$G(s) = \frac{k_{s,i} e^{-sT_d}}{s(s+K_2)}, \tag{18}$$

where T_d is the time delay in the system input. And K_2 is the additional damping coefficient.

The discretized state space equations are derived from Equation (18). With one additional state, the input error, a Kalman AOB [2] is designed to estimate the states of the system. The estimate of the input error is then directly cancelled at the input command (see Figure 3). Full state feedback is realized with the estimated state. Since most manipulators do not have torque sensors at each joint, it is not certain how accurately the input torque command is applied to the corresponding joint. This fact is one of the major model uncertainties in the system. Thus, the estimate of the input error plays an important role in actual manipulators.

The discretized state space form of the system equation (18) is

$$\begin{aligned} x_{r,k} &= \Phi_r x_{r,k-1} + \Gamma_r u_{k-1} \\ y_k &= C_r x_{r,k}, \end{aligned} \tag{19}$$

where u is the input command, $f^*_{c,i}$, and y is the output, $f_{c,i}$. The subscript i is omitted in the state space form since the system equation is the same for all the contacts.

[3]Stabilizing with only the estimate of the derivative of the contact force is not enough in practice; thus, additional damping with velocity measures are added.

With an input error estimate p_k,

$$\begin{aligned} x_{a,k} &= \Phi_a x_{a,k-1} + \Gamma_a u_{k-1} + \xi_k \\ y_k &= C_a x_{a,k} + \eta_k, \end{aligned} \tag{20}$$

where

$$x_{a,k} = \begin{bmatrix} x_{r,k} \\ p_k \end{bmatrix} \quad , \quad \Phi_a = \begin{bmatrix} \Phi_r & \Gamma_r \\ 0 & 1 \end{bmatrix} \tag{21}$$

$$\Gamma_a = \begin{bmatrix} \Gamma_r \\ 0 \end{bmatrix} \quad , \quad C_a = [C_r \quad 0] \tag{22}$$

and the stochastic inputs ξ_k and η_k are model and measurement uncertainties.

A full state feedback gain, L_r, is designed using pole placement method(Ackermann's formula). Combining the state feedback with the direct compensation of the input error estimate, the input to the system is

$$u_{k-1} = r_{k-1} - L_a \hat{x}_{a,k} \tag{23}$$

$$L_a = [L_r \quad 1]. \tag{24}$$

The state estimation is based on (20) and (23).

$$\hat{x}_{a,k} = \hat{x}_{a,k|(k-1)} + K_k(y_k - \hat{y}_k) \tag{25}$$

$$\hat{x}_{a,k|(k-1)} = \Phi_{a,closed} \hat{x}_{a,k-1} + \Gamma_a r_{k-1} \tag{26}$$

$$\Phi_{a,closed} = \begin{bmatrix} \Phi_r - \Gamma_r L_r & 0 \\ 0 & 1 \end{bmatrix} \tag{27}$$

$$\hat{y}_k = C_a \hat{x}_{a,k|(k-1)} \tag{28}$$

The Kalman gain K_k is

$$K_k = P_{1k} C_a^T [C_a P_{1k} C_a^T + R_k]^{-1} \tag{29}$$

with

$$P_{1k} = \Phi_a P_{k-1} \Phi_a^T + Q_k \tag{30}$$

$$P_k = P_{1k} - K_k C_a P_{1k}. \tag{31}$$

The system noise matrix, Q_k, represents model uncertainty. The term R_k is the measurement noise variance matrix. The term P_k is the mean square error matrix of the states.

Variance of noise measurement is one of the most important parameters in the Kalman filter design. However, the characteristic greatly changes for different contact conditions, e.g. moving contact or static contact. Therefore, on-line calculation of the variance of force measurement is conducted [8].

IV. Experiments

A. Experimental Setup

The experimental setup is shown in Figure 4. The PUMA560 manipulator is running at a servo rate of 500 Hz on a PC with QNX operating system. Contact forces are measured by JR3 force sensors.

The input time delay, T_d, is 3 sampling period. Due to this delay, $x_{a,k}$ in Equation (20) has 6 states that are contact force, the derivative of the contact force, 3 delayed inputs, and p_k. The system noise matrix, Q_k, and the initial mean square error matrix of the states, P_0, were set to $10^{-3} I_{6\times 6}$. The measurement noise variance, R_k, was estimated on-line using the previous 50 samples.

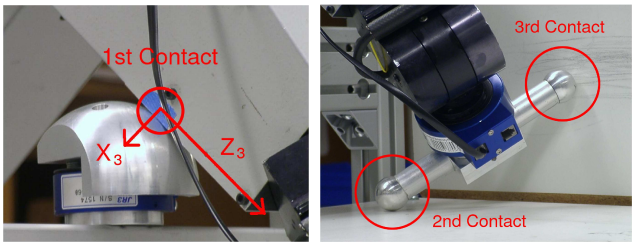

(a) (b)

Fig. 4. **System Setup.** (a) The third link having contact (b) The end-effector having two contacts

The first contact was established at the third link and the control point was chosen to be the contact point. The desired contact force direction was normal to the link, i.e. X_3 direction in Figure 4 (a). A JR3 force sensor was mounted on the contact environment. The contact force was computed by projecting the measured contact force to the normal direction of the contact link. The second and third contacts were at the end-effector; one contact with the horizontal table and the other with the vertical rigid board in Figure 4 (b). The control point of the end-effector was chosen to be the wrist point and another JR3 force sensor was mounted on the wrist.

The contact environments were an aluminium frame, a wooden table and a wooden vertical board. Consequently, they were near rigid contacts. However, the linkage between the table and the vertical board had some flexibility. The system stiffnesses of the three contacts were pre-estimated at low contact forces as $k_{s,1} = 6,000N/m$ for the third link contact, $k_{s,2} = 6,000N/m$ for the end-effector contact with the table, and $k_{s,3} = 3,000N/m$ for the end-effector contact with the vertical board. The actual stiffnesses of all three contacts were infinite at high contact forces. These estimates of the stiffness were used in the Kalman filter. The robustness of the controller with respect to the mismatch of the stiffness is studied in [2].

The motion control for the first control point was designed to hold the position along the third link, i.e. Z_3 in Figure 4 (a). The orientation of the end-effector was controlled through the null space control so that 2 remaining DOF could be controlled after controlling three contact forces and one motion direction. Two sets of experiments were conducted with and without motion command in the null space.

B. Static contact experiment (Figure 5- 7)

While three contact forces were controlled, the motion control was commanded to hold the current configuration. Since all three contacts were very stiff, the motion of the robot was very small during the experiment. When one of the desired contact forces was commanded with step functions, the other desired contact forces were controlled to be maintained at the same value.

Although the effect of one contact force control on the others was not perfectly eliminated, contact force control was successfully accomplished. The settling time of the

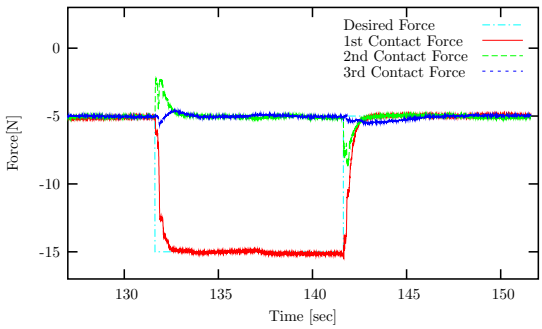

(a) Contact force measurement

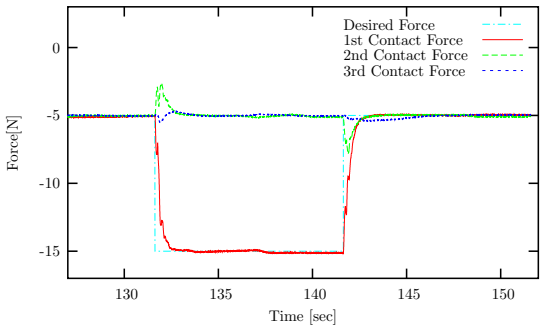

(b) Estimated contact force from Kalman filter

Fig. 5. **Static contact experiment.** Step response of the third link contact (1st contact).

step response was longer than the designed value (0.23 seconds) mainly due to the interaction with the other contact force controls. At the time of a step command, the contact force control corresponding to the step command created disturbance to the other contact forces, whose controller, then, compensated the disturbance. In the process, all three contact forces were affecting each other since the model of the manipulator and the contact environment was not perfect.

C. Moving contact experiment (Figure 8- 10)

Three contact forces were controlled to follow step commands from 5 to 15 N and the displacement along the third link was commanded to maintain the position. Concurrently, the desired orientation of the end-effector was designed to rotate around the 4th joint of PUMA560, i.e. the first joint of the wrist. Therefore, the second and third contact points moved along the table and vertical board correspondingly. The first contact at the third link also moved in the direction that was perpendicular to the direction along the link and the contact direction. That is, the contact point moved in Y_3 direction in Figure 4 (a).

All three contact forces were affected by the wrist motion mainly due to the contact surface characteristics and imperfect kinematic model of the contact. Especially, when the contact started moving, greater disturbance was produced to contact forces due to the static friction of the contacts.

Although the measurement characteristic changed from static contact to moving contact, the robust force controller

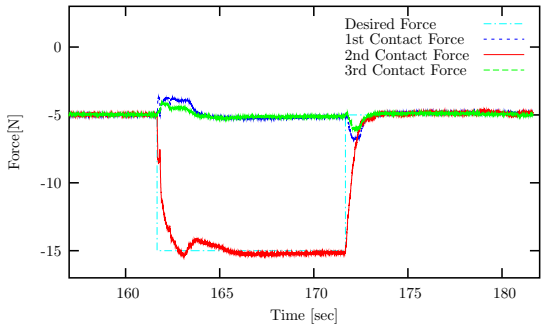

(a) Contact force measurement

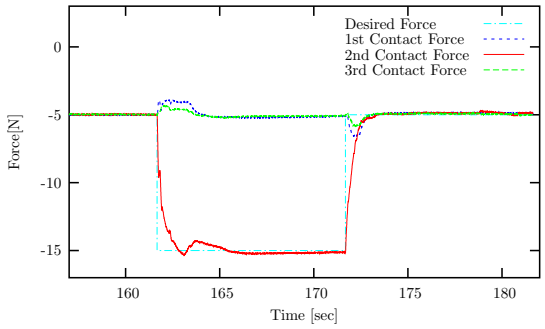

(b) Estimated contact force from Kalman filter

Fig. 6. **Static contact experiment.** Step response of the end-effector contact with the horizontal table (2nd contact).

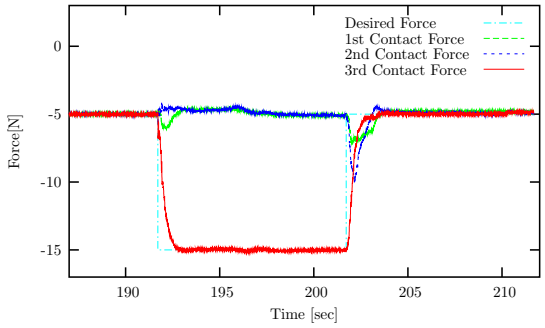

(a) Contact force measurement

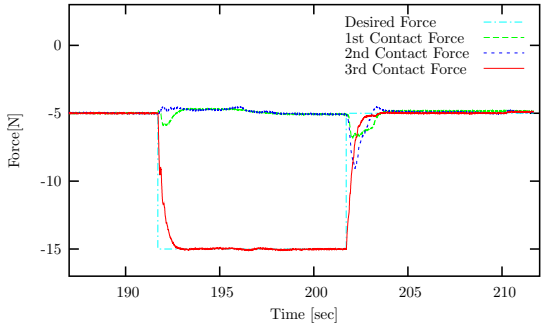

(b) Estimated contact force from Kalman filter

Fig. 7. **Static contact experiment.** Step response of the end-effector contact with the vertical board (3rd contact).

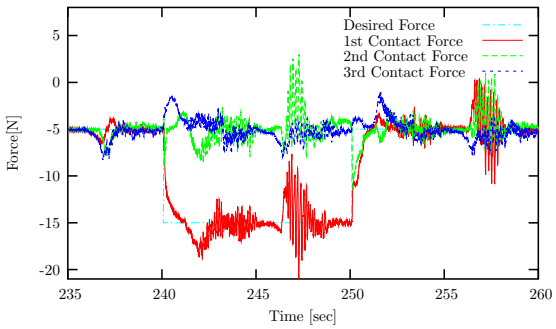

(a) Contact force measurement

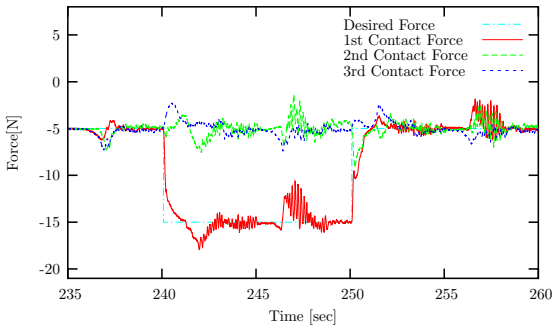

(b) Estimated contact force from Kalman filter

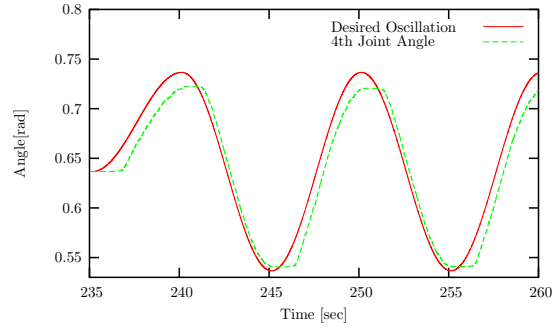

(c) 4th joint motion

Fig. 8. **Moving contact experiment.** Step response of the third link contact (1st contact).

with on-line variance estimation maintained the contact forces while rejecting the disturbances.

V. Conclusion

A framework for multi-link multi-contact compliant motion control is presented in this paper. The complex contact compliant task is implemented in the operational space formulation utilizing a multi-contact model and contact environment model. The operational space coordinates are defined to be the composition of the displacements in the contact normal spaces. To effectively deal with modeling errors, full state feedback with a Kalman active observer is applied. Motion is controlled in the null space of the contact force space.

The experimental results demonstrate the successful implementation of the framework for three point contact control; one with the third link and two with the end-effector of the PUMA560 manipulator. Static and moving contact

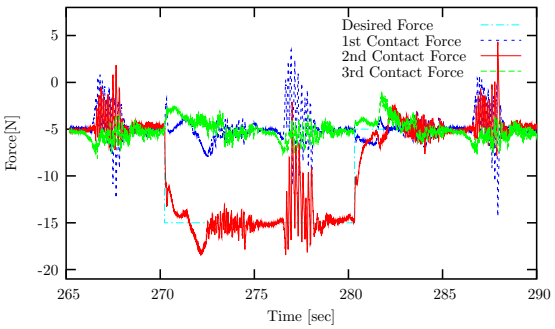

(a) Contact force measurement

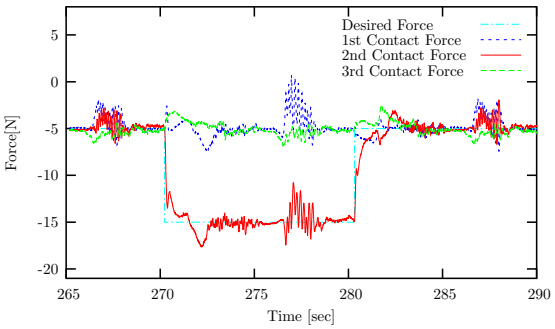

(b) Estimated contact force from Kalman filter

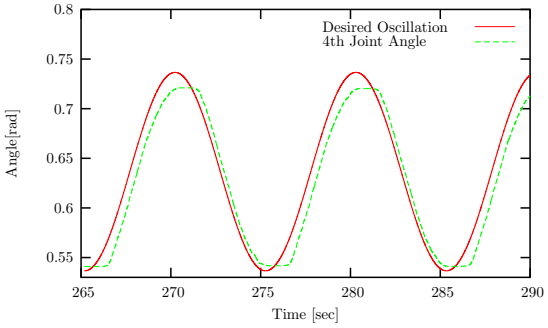

(c) 4th joint motion

Fig. 9. **Moving contact experiment.** Step response of the end-effector contact with the horizontal table (2nd contact).

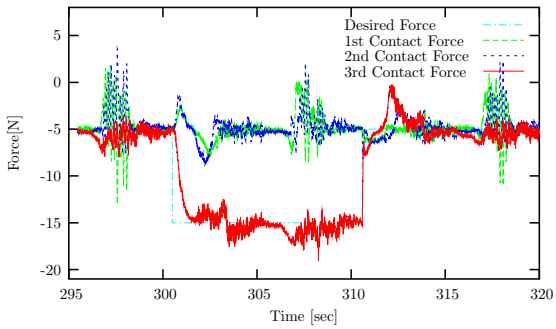

(a) Contact force measurement

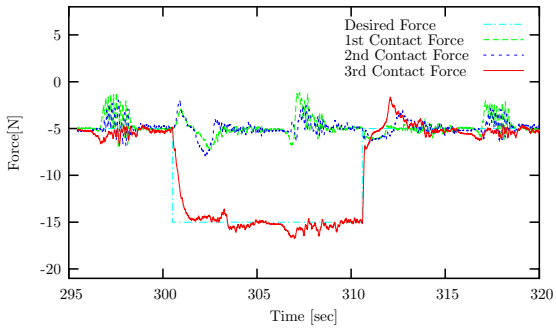

(b) Estimated contact force from Kalman filter

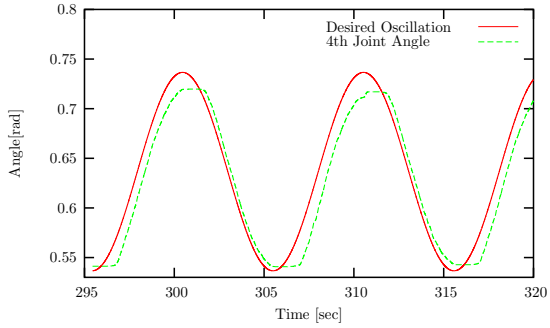

(c) 4th joint motion

Fig. 10. **Moving contact experiment.** Step response of the end-effector contact with the vertical board (3rd contact).

experiments show the high performance of the multi-link multi-contact force control framework even in the presence of varying contact characteristics and disturbance from the motion of the manipulator.

ACKNOWLEDGMENT

The authors would like to acknowledge Peter Thaulad for his contributions to the setup of hardware in the experiments.

REFERENCES

[1] H. Bruyninckx, S. Demey, S. Dutré, and J. De Schutter. Kinematic models for model-based compliant motion in the presence of uncertainty. *Int. J. of Robotics Research*, 14(5):465–482, Oct 1995.

[2] R. Cortesão, J. Park, and O. Khatib. Real-time adaptive control for haptic manipulation with active observers. In *Proc. of the Int. Conf. on Intelligent Robots and Systems (IROS)*, Las Vegas, 2003.

[3] R. Featherstone, S. Thiebaut, and O. Khatib. A general contact model for dynamically-decoupled force/motion control. In *Proc. of the Int. Conf. on Robots and Automation*, pages 3281–3286, 1999.

[4] O. Khatib. A unified approach for motion and force control of robot manipulators: The operational space formulation. *Int. J. on Robotics and Automation*, 3(1):43–53, February 1987.

[5] O. Khatib and J. Burdick. Motion and force control of robot manipulators. In *Proc. of the Int. Conf. on Robotics and Automation*, pages 1381–1386, 1986.

[6] H. Lipkin and J. Duffy. Hybrid twist and wrench control for a robotic manipulator. *ASME Journal of Mechanisms, Transmissions and Automation in Design*, 110(2):138–144, Jun 1988.

[7] Y. Liu, K. Kitagaki, T. Ogasawara, and S. Arimoto. Model-based adaptive hybrid control for manipulators under multiple geometric constraints. *IEEE Trans. on Control Systems Technology*, 7(1):97–109, January 1999.

[8] J. Park, R. Cortesão, and O. Khatib. Multi-contact compliant motion control for robotic manipulators. In *Proc. of the Int. Conf. on Robotics and Automation*, New Orleans, U.S.A., 2004.

[9] M. H. Raibert and J. J. Craig. Hybrid position/force control of manipulators. *ASME Journal of Dynamic Systems, Measurement and Control*, 103(2):126–133, June 1981.

[10] H. West and H. Asada. A method for the design of hybrid position/force controllers for manipulators contrained by contact with the environment. In *Proc. of the Int. Conf. on Robotics and Automation*, pages 251–259, 1985.